HAL
open science

Nucleation control in precipitation processes by ultrasound

Cendrine Gatumel, Fabienne Espitalier, Jacques Schwartzentruber, Béatrice Biscans, Anne Marie Wilhelm

To cite this version:

Cendrine Gatumel, Fabienne Espitalier, Jacques Schwartzentruber, Béatrice Biscans, Anne Marie Wilhelm. Nucleation control in precipitation processes by ultrasound. Kona, 1998, 16, p. 160-169. hal-01845417

HAL Id: hal-01845417

https://hal.science/hal-01845417

Submitted on 10 Sep 2018

HAL is a multi-disciplinary open access archive for the deposit and dissemination of scientific research documents, whether they are published or not. The documents may come from teaching and research institutions in France or abroad, or from public or private research centers.

L'archive ouverte pluridisciplinaire **HAL**, est destinée au dépôt et à la diffusion de documents scientifiques de niveau recherche, publiés ou non, émanant des établissements d'enseignement et de recherche français ou étrangers, des laboratoires publics ou privés.

Nucleation Control in Precipitation Processes by Ultrasound

C. Gatumel, F. Espitalier, and J. Schwartzentruber
*Ecole des Mines d'Albi**
B. Biscans and A.M. Wilhelm
*ENSIGC-LGC Toulouse***

Abstract

The effect of an ultrasonic field on the precipitation process of barium sulphate has been investigated.

Experiments in a semi-batch precipitator showed that small crystal sizes with narrow distribution are obtained with ultrasound in a very reproducible way; however, this effect could not be assigned to an improvement in micromixing.

Experiments on continuous precipitation of barium sulphate in two reactors in series were carried out in order to characterise the effect of ultrasound on precipitation, by separating the nucleation and growth processes. It was concluded that the main effect of ultrasound is an enhancement of secondary contact nucleation by acoustic cavitation.

This change in the precipitation process allows small crystals with uniform size and shape to be obtained without effect of mechanical mixing. It is only necessary to sonicate the mixing volume of the reactants with a low level of ultrasonic power: this is very promising for industrial applications.

1. Introduction

The quality of particles produced by precipitation is largely determined by the very fast nucleation step, and is therefore difficult to control in industrial processes. Nucleation in precipitation depends strongly on the way the reactants are put into contact (1). In general, this results in a non-reproducible polymodal particle size distribution which makes it necessary to carry out sieving, grinding or agglomeration to obtain the required particle size.

It is well known that power ultrasound causes unstable cavitation in liquids, resulting in violent collapse of cavitation bubbles; therefore, ultrasound is expected to improve the micromixing of the liquid reactants (2), thus giving better control of supersaturation and nucleation. In addition, ultrasound can have effects on the solid particles by erosion and desaglomeration (3).

The main objective of this work was to investigate the role of ultrasound in the precipitation of a model product: barium sulphate. We divided this investigation into two parts. At first, we studied a semi-batch precipitation with micromixing characterisation. In a second phase, the direct effects of ultrasound on nucleation and growth were shown in a continuous precipitation. And finally, we tried to highlight the most important parameters in ultrasound-enhanced precipitation.

* Route de Teillet, 81013 Albi, France
**Chemin de la Loge, 31078 Toulouse, France

2. Materials and methods

2.1 Experimental apparatus

We studied the precipitation of barium sulphate at 20°C in accordance with the following equation:

$$Na_2SO_4 + BaCl_2 \rightarrow BaSO_4 \downarrow + 2NaCl$$

The solvent was demineralized water. The reactant concentration was chosen so as to avoid agglomeration: 1 mol/m^3 after mixing of reactants.

In both cases ultrasound is emitted directly in the solution. The frequency is 20 kHz, and the power involved is between 30 and 220 W. Under these conditions, ultrasound causes acoustic cavitation in liquids.

The ultrasound power levels reported in our experiments always signify the electrical power consumed by the generator, as measured with a wattmeter. The power dissipated in the liquid medium can be estimated by calorimetry. We found that the dissipated power is only 40% of the electrical power consumed by the generator.

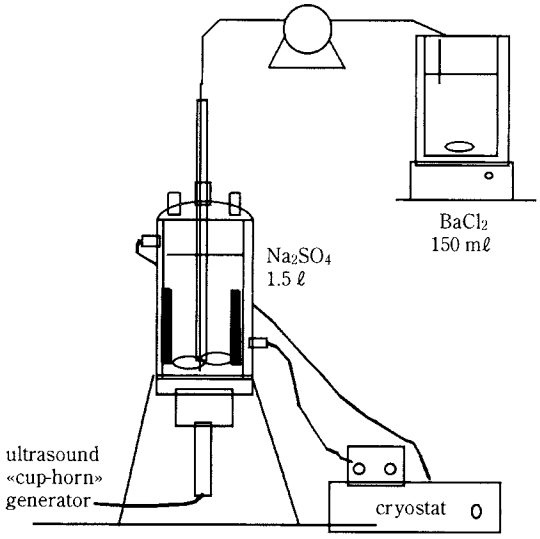

Fig. 1 Experimental equipment for semi-batch precipitation

2.1.1 Semi-batch precipitation

Figure 1 shows the apparatus used to study the semi-batch precipitation. The precipitator is baffled reactor, stirred with a marine propeller. Stirring speed is between 200 and 1000 rpm. Ultrasound is emitted directly into the liquid at the bottom of the reactor.

A solution of sodium sulphate (1.5 ℓ) is already in the reactor. Barium chloride (150 mℓ) is added by means of an inlet tube located in the stirrer spindle. Under these conditions, reactants are mixed just above (2 cm) the ultrasound emitter, so that the nucleation zone is well sonicated.

2.1.2 Continuous precipitation

The equipment consists of two reactors in series (see **Figure 2**). Each reactor can be sonicated separately. The first one is a small, stainless steel cell (0.05 ℓ) where nucleation is expected to be the dominant process. Ultrasound is emitted by means of a probe inside the cell. Reactants are introduced through a coaxial tube and mixed just under the ultrasonic probe. The second reactor is a one-litre, stirred reactor with baffles, and ultrasound emitted at the bottom (similar to the semi-batch reactor described in section 2.1.1); a longer residence time allows particles to grow. The stirrer speed in the growth reactor is 440 rpm and the total flow rate is 480 mℓ/min.

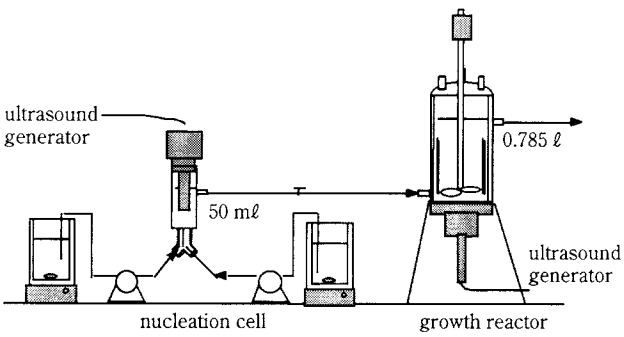

Fig. 2 Experimental equipment for continuous precipitation

2.2 Characterisation of the micromixing in the semi-batch reactor

The mixing of two miscible fluids can be analysed in terms of **macromixing** (dispersion of aggregates from one fluid into the other) and **micromixing** (molecular scale mixing of the reactants). The micromixing level was determined using the Bourne reaction (4) (a diazo coupling reaction involving consecutive competitive reactions):

$$A+B \rightarrow p\text{-}R \quad (1)$$
$$A+B \rightarrow o\text{-}R \quad (2)$$
$$p\text{-}R+B \rightarrow S \quad (3)$$
$$o\text{-}R+B \rightarrow S \quad (4)$$

where A is 1-naphthol, B is diazo sulphanilic acid, p-R and o-R are mononitric dyes, and S is a bi-nitric dye. Initial concentrations are chosen to give a slight excess of A with respect to B. The solution of A is already present in the reactor, and B is introduced slowly.

In the case of bad micromixing, aggregates of B remain in solution, so that the p-R or o-R formed by reactions (1) and (2) are still in contact with unreacted B: there is a high conversion of B into S. On the other hand, if the micromixing is good, very little S is produced.

The segregation index is defined as:

$$X_s = \frac{2C_s}{2C_s + C_{o-R} + C_{p-R}}$$

Reactions (1) and (2) are instantaneous, and (3) and (4) are very fast. X_S is close to unity for a very bad micromixing and will tend towards zero if micromixing is perfect.

2.2.1 Experimental procedures

The reaction is performed in the semi-batch apparatus described in section 2.1.1. The reactor contains initially 1.5 ℓ of solution 1-naphthol (0.527 mol/m^3) buffered a pH=10, and 150 mℓ of a solution of diazotised sulphanilic acid (5 mol/m^3) are added in 10 minutes.

The concentrations of the products are determined by spectrophotometry in the visible range. We used the molar absorption coefficients of the three dyes determined by Wenger et al (5).

2.2.2 Calculation of the mixing times

The Segregated Feed Model (SFM) developed by Villermaux (6) was adapted to a simple jet feed in

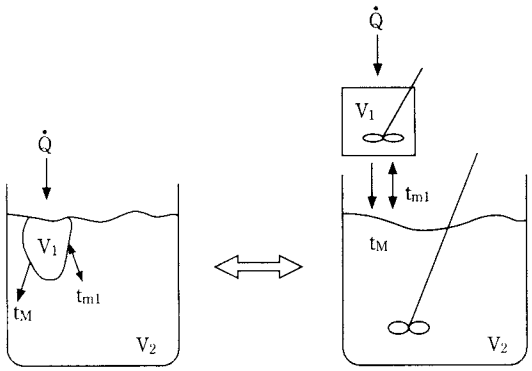

Fig. 3 Principle of SFM model for a simple jet reactor

order to deduce the mixing times from the measured segregation index.

This phenomenological model takes into consideration that the reactor is divided into two zones (see **Figure 3**). Each zone is a perfectly mixed reactor. We considered two different types of mass transfer between these two zones:

- an irreversible transfer from the feed to the reactor volume. This is the macromixing and its characteristic time is t_M.
- a reversible transfer between the two zones, which represents the micromixing and its characteristic time is t_m.

The corresponding set of ordinary differential equations is solved numerically (see appendix 1). This model allows calculation of the dye concentrations and the segregation index X_S from t_M and t_m. Reciprocally, it is possible to fit values of mixing times t_M and t_m to measured dye concentrations by means of a standard parameter estimation method.

2.3 Precipitation characterisation

Following a precipitation requires knowing both the solution composition and the solid product characteristics.

2.3.1 Solution

As the reaction is performed with salts, we can measure the concentration of unreacted species in the precipitation by conductimetric measurements. The mean relative supersaturation can be calculated with:

$$S=\frac{C_{BaSO_4}}{\sqrt{K_S}}\cdot\gamma\pm$$

K_S: solubility product; C_{BaSO4} is the concentration of $BaSO_4$; $\gamma\pm$ is the mean activity coefficient. It is calculated with the Bromley equations for an electrolyte (7).

2.3.2 Solid product

At the end of the experiments, crystal size distributions are measured with a Malvern Mastersizer laser diffraction instrument. The samples are taken and analysed immediately and without dilution. We can also filter a sample of solution and observe the crystals' shape with a Scanning Electron Microscope.

3. Results and discussion

3.1 Investigations of the role of mixing during the semi-batch sonicated precipitation

We first investigated the influence of mixing conditions on the precipitation of barium sulphate. Experiments were conducted in the semi-batch equipment. At first, we determined that, under the experimental conditions we used, macromixing was not a limiting step. We therefore present only the study of micromixing in the experimental apparatus.

3.1.1 Effect of ultrasound on micromixing

The micromixing level in the precipitator subjected to ultrasound was determined as a function of the stirrer speed in a liquid phase without precipitation. Very similar results were obtained in a synthetic liquid-solid suspension, showing that the presence of solid particles does not significantly affect the micromixing (8).

In **Figure 4**, we report the segregation index obtained by the Bourne characterisation method for several stirrer speeds and ultrasonic power levels. For the lowest agitation levels, micromixing is improved by an increase of the ultrasonic power, but this effect of ultrasound on micromixing disappears at high stirrer speeds. Similar results have been obtained by other authors (9), and could be explained by an interaction between turbulence and cavitation caused by high-speed stirring and the acoustic waves propagation.

It can be noticed that our segregation indexes

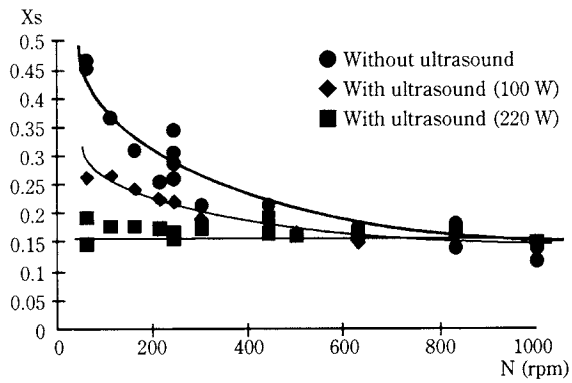

Fig. 4 Influence of stirrer speed and ultrasound on the segregation index

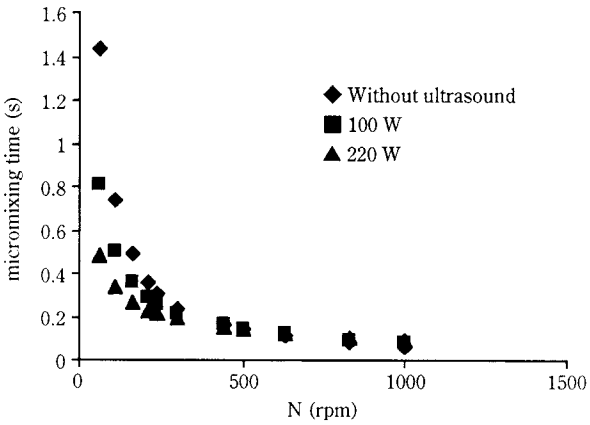

Fig. 5 Micromixing times calculated from the segregation indexes

remain rather high, and that the best micromixing is obtained at a high stirrer speed: 600 rpm for a 2-litre reactor. This is probably because the reactants are introduced at a very low point in the reactor (just above the ultrasound transducer).

We have noticed that the results are more reproducible with ultrasound. The mixing times calculated from the micromixing experiments are shown in **Figure 5**. In all our experiments, the micromixing times were larger than 0.05 s. On the one hand, these values are much larger than the characteristic time of the Bourne reaction (10^{-5} second), which means that this reaction is really controlled by micromixing in our experimental conditions, even for the highest agitation levels. And on the other hand, the mixing times are greater than the characteristic time of precipitation (induction time) which is of the order of magnitude of 10^{-3} second. This confirms that precipitation should be affected by micromixing conditions, since nucleation will occur before mixing is complete.

3.1.2 Effect of ultrasound on the precipitation product

The precipitates formed both with and without ultrasound were compared for shape and particle size distribution. **Figure 6** shows photographs of crystals.

Without ultrasound, there are some platelets topped with crystallites, and some "roses of the desert". These last ones do not seem to be agglomerates of platelets, but probably platelets which have grown on top of each other.

When precipitation is carried out under ultrasonic irradiation, crystals are smaller but they still have the same shape. It may be concluded that the presence or absence of ultrasound does not change the morphology of particles.

Figure 7 shows the particle size distributions obtained for several ultrasonic powers at 240 and 1000 rpm. For both agitation speeds, ultrasound leads to a reduced crystal size and a narrower particle size distribution. It was also observed that our results are much more reproducible in the presence of ultrasound.

The mean crystal size obtained for several ultrasonic powers are reported as a function of the stirrer speed in **Figure 8**.

Without ultrasound, when the stirrer speed is increased, the mean particle size seems to remain constant or to increase slightly between 200 and 600 rpm, and then decreases. This shows the importance and complexity of mixing phenomena during precipitation. These results suggest that the production of supersaturation is controlled by the contacting of reactants, and thus by the micromixing conditions. At low stirrer speeds, reactants are badly mixed, local supersaturation is quite low, few nuclei are formed and the mean supersaturation is high enough to

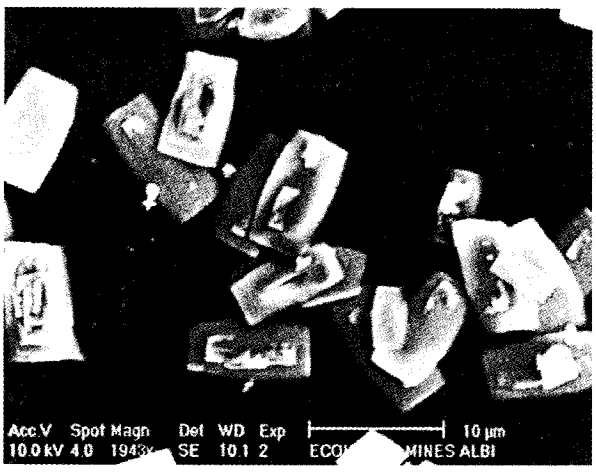

Without ultrasound

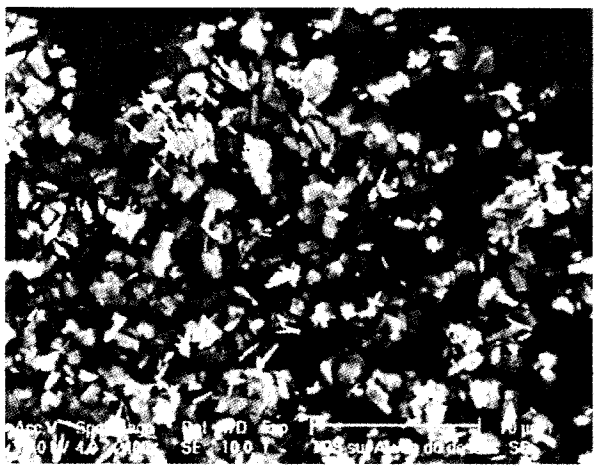

200 Watt

Fig. 6 Crystal shapes observed with a S.E.M. microscope for precipitation with or without ultrasound

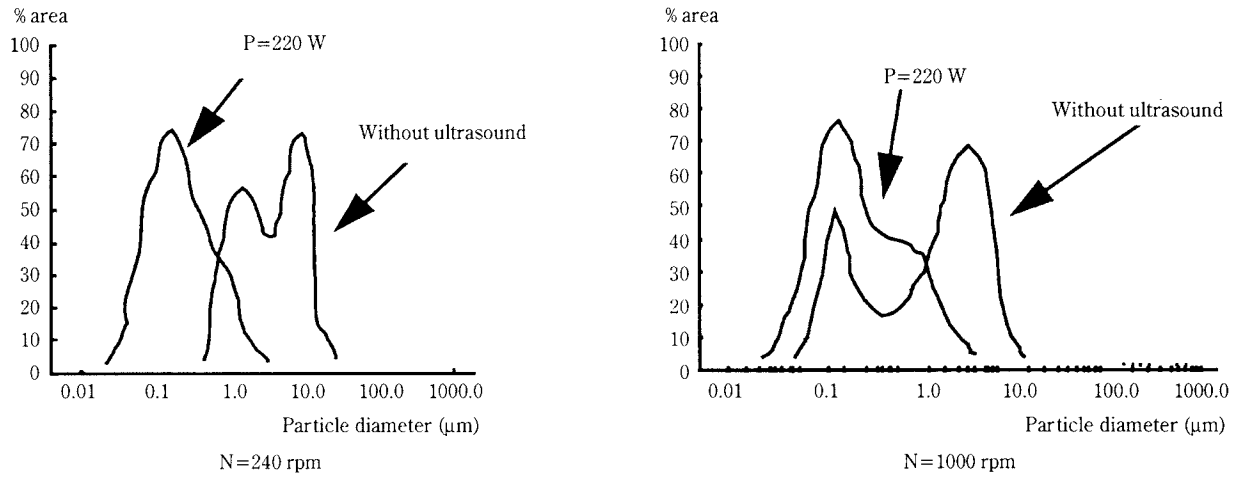

Fig. 7 Influence of ultrasound on particle size distribution (in surface) for two stirrer speeds

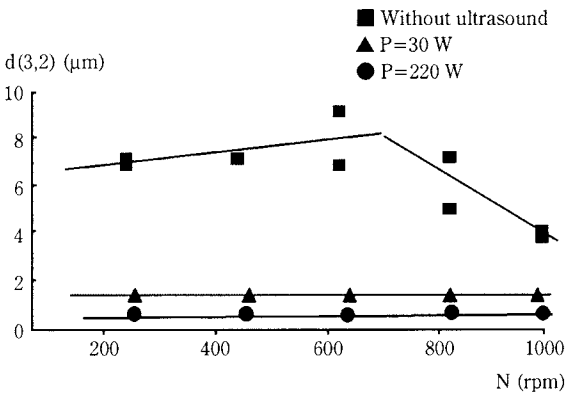

Fig. 8 Influence of stirrer speed and ultrasound on the mean particle size of crystals

permit crystal growth. Improving the mixing will enhance both crystal growth and nucleation, and there is no clear effect of mixing on particle size. But, when local mixing in the nucleation zone is sufficient, local supersaturation increases, resulting in abundant nucleation and a strong decrease in crystal size. We conclude from these results that without ultrasound, the precipitation process seems to be very sensitive to the mixing conditions in the reactor.

In the presence of ultrasound, **Figure 8** shows that for all stirrer speeds, the mean crystal size decreases with increasing ultrasonic power; considering the resolution of the particle size analysis, there is no significant effect of stirrer speed on the mean particle size.

As a first conclusion, we can see that the effects of the micromixing conditions disappear in the presence of ultrasound. Moreover, one can see (Figure 4) that when the stirrer speed is greater than 600 rpm, the micromixing index is the same with and without ultrasound; however, the mean crystal size is strongly affected by ultrasound.

This shows that the effect of ultrasound on precipitation is not due to an improvement in micromixing, but there must be a specific effect of ultrasound on the precipitation mechanisms, namely nucleation or growth, since there is no agglomeration in our experiments.

3.2 Ultrasound effect on nucleation

In order to determine the influence of ultrasound on nucleation and growth, we chose to work in continuous mode by physically separating these two processes. The experimental device is described in 2.1.2. Reported mean sizes are calculated from the size distribution on the surface. Numbers of particles are given for 100 mℓ of suspension. These last quantities could not be determined with great precision and should be considered only as orders of magnitude. The ultrasonic power used in these experiments was 200 W.

3.2.1 Ultrasound in the nucleation cell

Results in terms of supersaturation, size and number are presented in **Table 1**. The shapes of crystals obtained in the cell without ultrasound and for 200 W are presented in **Figures 9-a** and **9-b**, respectively.

Without ultrasound, crystals are in the form of "roses of the desert" and platelets, and they are topped with growing crystallites. With ultrasound there are only platelets, and no more crystallites.

Table 1 Ultrasound effect in the nucleation cell

	without ultrasound	200 Watt
Supersaturation	46.5	15.2
mean size (μm)	4.1	0.9
number for 100 mℓ	~1e10	~1e11

Ultrasound allows the creation of more and smaller crystals. But these crystals do not seem to be broken crystals, and the final supersaturation is divided by two when ultrasound is used. The effect of ultrasound in the cell is clearly an increase of nucleation rate (primary or secondary).

3.2.2 Ultrasound in the growth reactor

Table 2 presents supersaturation, size and number of crystals obtained in the growth reactor, either with or without ultrasound in the cell. **Figures 9-c** and **9-d** represent the shape of crystals formed with and without ultrasound in the growth reactor, when there is no ultrasound in the nucleation cell.

If ultrasound is applied to the cell, supersaturation at the exit of the cell is very low (lower than 15), and so there is not much solute remaining to nucleate or to feed the crystals by growth. The number of particles is the same in both reactors; supersaturation is slightly lower in the growth reactor and the mean size is slightly larger.

If neither the cell nor the growth reactor is sonicated, values in **Table 2** indicate that there is only growth and no nucleation in the growth reactor. As in the cell, Figure 9-c shows that crystals present platelets and "roses of the desert" shapes. The difference is that there are more crystallites on the crystals.

If the growth reactor only is sonicated (200 W), one sees that supersaturation and mean crystal size are smaller in the growth reactor than in the cell, and that there are more crystals in the growth reactor. Crystal shapes are mainly platelets, with some "roses of the desert" shape (see Figure 9-d). But as in the cell with

Table 2 Ultrasound effect in the growth reactor

Ultrasonic power in the nucleation cell	Ultrasonic power in the growth reactor	supersaturation n	mean size (Nm)	number for 100 mℓ
0 W	0 W	26.4	6.9	~1e10
0 W	200 W	16	0.80	~1e11
200 W	0 W	10.4	0.80	~1e11
200 W	200 W	10.2	0.85	~1e11

a 9 μm

Nucleation without ultrasound

b 9 μm

Nucleation with ultrasound (200 W)

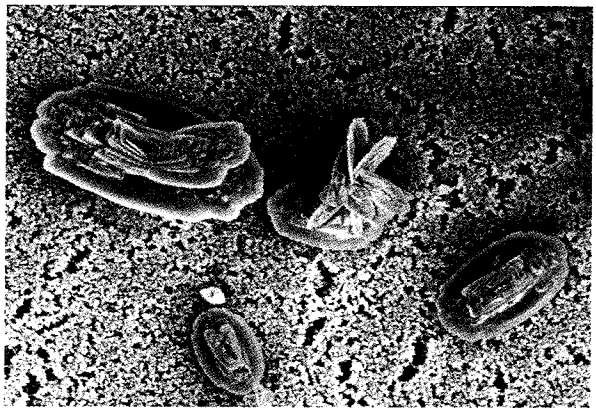

c 32 μm

Growth without ultrasound

d 9 μm

Growth with ultrasound (200 W)

Fig. 9 Ultrasound effect on crystal shape in the continuous reactors

ultrasound, they are not topped with crystallites any more. In this case, it seems that creation of crystals in the growth reactor is not due to breakage but to nucleation.

3.2.3 Proposed mechanism

Results obtained with the continuous sonicated precipitators show that ultrasound has a strong effect on nucleation. As far as very small supersaturations are concerned (only 10 in the growth reactor with ultrasound when there is no ultrasound in the cell), it may be secondary nucleation. The probable mechanism could be contact nucleation (10): when a cavitation bubble implodes near a growing crystal, it can remove clusters forming on a crystal surface or petals of roses in formation and thus produce new nuclei in solution.

3.3 Validation by the population balance

The two reactors in series were modelled on the basis of a simple population balance. They are supposed to be MSMPR (Mixed Suspension Mixed Product Removal), and we have chosen to describe the growth rate as being dependent on the crystal size. The model equations are presented in appendix 2. The kinetic parameters have been fitted to experimental crystal size distributions. These calculations should not be considered as a precise quantitative study, but rather as a tool to determine tendencies in order to validate our assumptions.

3.3.1 Nucleation at the "zero size"

At first, we assumed that secondary nucleation was contact nucleation rather than breakage. In the population balance, this could be expressed by nucleation at the "zero size", which is equivalent to the first class of crystals. The computed nucleation rates are reported in **Tables 3** and **4** for the nucleation cell

Table 3 Nucleation rate values in the cell calculated by population balance

	B, crystals/m^3/s
cell without ultrasound	1.22 e 15
cell with 200 Watt	3.53 e 15

Table 4 Nucleation rate values in the growth reactor calculated by population balance, crystals/m^3/s

	Growth reactor without ultrasound	Growth reactor 200 Watt
cell without ultrasound	0	9 e 13
cell 200 Watt	0	0

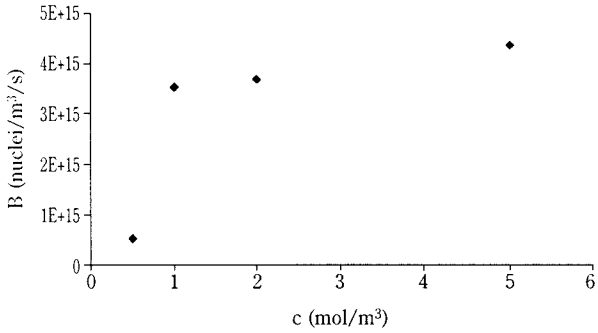

Fig. 10 Nucleation rate in the small cell as a function of the initial concentration

and the growth reactor. These values allow good representation of the experimental size distributions. This shows that nucleation occurs at the minimum crystal size and can therefore be primary or secondary contact nucleation. The method cannot discriminate between these assumptions; however, secondary nucleation is more likely to occur in an ultrasonic field.

3.3.2 Influence of initial concentration

We calculated nucleation rates in the small cell subjected to ultrasound (200 W) for different initial concentrations: 0.5 mol.m^{-3}, 1 mol.m^{-3}, 1.5 mol.m^{-3}, and 2 mol.m^{-3}. The results are plotted in **Figure 10**. The nucleation rates depend on initial concentrations. This reinforces the hypothesis of secondary contact nucleation (10), since the breakage nucleation rate should be independent of supersaturation.

4. Influence of the ultrasonic parameters on the crystal's characteristics during the continuous precipitation process

We found that the most important effect of ultrasound in the precipitation of barium sulphate is to cause secondary nucleation. Characterisation of the ultrasound effect on the process requires knowing the influence of the power involved and the ultrasound location. We ran experiments by separately sonicating the cell and the growth reactor with different powers. The values observed are the mean crystal size and the number of crystals in the cup-horn. The results are reported in **Figure 11**.

In terms of final product number and size, applying ultrasound to the small cell or to both reactors leads to the same results and the ultrasonic power does not seem to have a significant effect. There are indications that a 100 W power level could be somewhat more efficient than 200 W. This is perhaps because

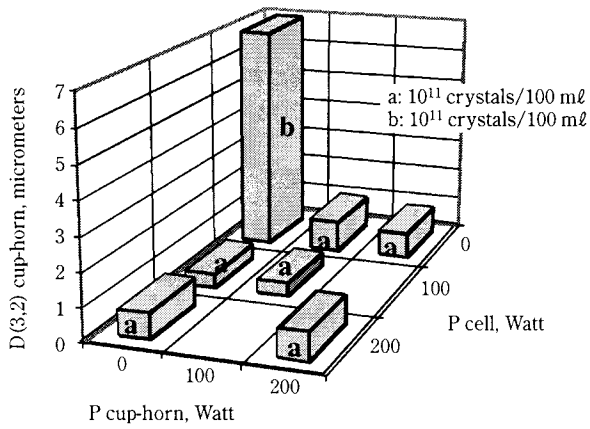

Fig. 11 Effects of ultrasound power and location on mean crystal size and number of crystals

when the ultrasonic power increases, the number of cavitation bubbles also increases, thus hindering the propagation of the acoustic wave. We also did some experiments at 50 W, which is the lowest power delivered by our ultrasound generator, and the results were essentially the same as for 100 W.

5. Conclusion

It has been shown that applying an ultrasonic field during barium sulphate precipitation leads to much more reproducible results. Without changing the morphology of the crystals, it brings about a large reduction in the mean particle size and a narrower size distribution.

These beneficial effects cannot be attributed to an improvement in reactant micromixing; it is demonstrated that ultrasound has a direct effect on the nucleation process (mainly on secondary contact nucleation), which is promoted by acoustic cavitation. These effects can be obtained with a low acoustic power, and it is only necessary to apply ultrasound in the small nucleation volume where the reactants are put into contact. Ultrasound therefore appears to be a very promising way of improving the control of industrial precipitation processes.

Nomenclature

a	: coefficient for growth rate	[m^{-1}]
B	: nucleation rate	[crystals/m^3/s]
C_i	: concentration of product i	[mol/m^3]
d(3,2)	: mean particle size (in surface)	[μm]
G	: growth rate	[m/s]
G_0	: growth rate at zero size	[m/s]
k	: kinetic constant	[m^3/mol.s]
L	: crystal size	[mm]
Q	: feed rate	[m^3/s]
n	: population density	[crystals/m^4]
r_{ij}	: production rate of component i in zone j	[mol/m^3.s]
t_M	: macromixing characteristic time	[s]
t_m	: micromixing characteristic time	[s]
t	: mean residence time	[s]
V_i	: volume of zone i	[m^3]
X_s	: segregation index	

References

1) GARSIDE. Tailoring crystal products in precipitation processes and the role of micromixing. AIChE Symposium series, 87(284), 16-25, 1991
2) OKADA, S. FUSEYA, Y. NISHIMURA, M. MATSUBARA. Effect of ultrasound on micromixing. Chem. Eng. Sci., 27(3), 529-535, 1972
3) LEBRAS. Action des ultrasons sur les processus physicochimiques. Revue de chimie minérale, 4, 283-315, 1967
4) BOURNE, F. KOSICKI and P. RYS. Mixing and fast chemical reaction1: test reaction to determine segregation. Chem. Eng. Sci., 36 (10), 1643-1648, 1981
5) WENGER, E.H. DUNLOP and I.D. MACGILP. Investigation of the chemistry of a diazo micromixing test reaction. A.I.Ch.E. Journal, 38 (7), 1105-1114, 1992
6) VILLERMAUX. A simple model for partial segregation in a semi-batch reactor. A.I.Ch.E. Annual Meeting, paper 114-A (1st page), A1-B2, 1989
7) BROMLEY. Thermodynamic properties of strong electrolytes in aqueous solution. A.I.Ch.E. Journal, 19, 313-320, 1973
8) GATUMEL, F. ESPITALIER, O. LOUISNARD, J. SCHWARTZENTRUBER, B. BISCANS and A.M. WILHELM. Micromixing and ultrasonic precipitation of barium sulphate. Proceedings of the ECCE-1 congress, vol. 2, P.1511, 1997
9) MONNIER, A.M. WILHELM and H. DELMAS. Ultrasonic mixing: preliminary results. A.I.Ch.E. Symposium series, San Diego, California, 214-219, 1996
10) GARSIDE and R.J. DAVEY. Secondary contact nucleation: kinetics, growth and scale-up. Chem. Eng. Com., 4, 393-424, 1979

Appendix 1

Differential equations system for the SFM model in the case of a simple jet reactor

$$A + B \rightarrow p - R,\ k_{1\text{-}p} = 12238$$
$$A + B \rightarrow o - R,\ k_{1\text{-}o} = 921$$
$$p - R + B \rightarrow S,\ k_{2\text{-}p} = 1.835$$
$$o - R + B \rightarrow S,\ k_{2\text{-}o} = 22.25$$

For zone 1 reaction rates are:

$$r_{A1} = -(k_{1\text{-}p} + k_{1\text{-}o})C_{A1}C_{B1}$$
$$r_{B1} = -(k_{1\text{-}p} + k_{1\text{-}o})C_{A1}C_{B1} - k_{2\text{-}p}C_{pR1}C_{B1} - k_{2\text{-}o}C_{oR1}C_{B1}$$
$$r_{pR1} = -k_{1\text{-}p}C_{A1}C_{B1} - k_{2\text{-}p}C_{R1}C_{B1}$$
$$r_{opR1} = -k_{1\text{-}o}C_{A1}C_{B1} - k_{2\text{-}o}C_{R1}C_{B1}$$

Equations for zone 2 are strictly analogous.
Volume balances are:

$$\frac{dV_1}{dt} = -\frac{V_1}{t_M} + Q$$
$$\frac{dV_2}{dt} = -\frac{V_2}{t_M}$$

Partial mass balances are:

$$\frac{d(V_1C_{i1})}{dt} = -\frac{V_1C_{i1}}{t_M} + \frac{V_1V_2}{V_1+V_2}\frac{C_{i2}-C_{i1}}{t_m} - r_{i1}V_1$$
$$\frac{d(V_2C_{i2})}{dt} = -\frac{V_1C_{i1}}{t_M} + \frac{V_1V_2}{V_1+V_2}\frac{C_{i1}-C_{i2}}{t_m} - r_{i2}V_2$$

Initial conditions

$t = 0$, $V_1 = 0$, and $V_2 = V_o$

Appendix 2

MSMPR population balance

Population balance in the nucleation cell:

$$\frac{n_1}{\tau_1} + \frac{d(n_1G_1)}{dL} = 0$$

with

$$n_1(L_0) = \frac{B_1}{G_0^1}$$

In the growth reactor:

$$\frac{n_2 - n_1}{\tau_2} + \frac{d(n_2G_2)}{dL} = 0$$

with

$$n_2(L_0) = \frac{B_2}{G_0^2}$$

Crystal growth rate (Canning and Randolph model, order 1):

$$G_i(L) = G_0^i(1 + a_iL)$$

After integration, the population balance in the cell becomes:

$$n_1 = n_0^1(1 + a_1L)^{-\frac{1+a_1G_0^1\tau_1}{a_1G_0^1\tau_1}}$$

with

$$n_0^1 = \frac{B_1}{G_0^1}$$

The equation for the growth reactor must be integrated numerically:

$$G_2(L)\frac{dn_2(L)}{dL} + n_2(L)\left(\frac{dG_2(L)}{dL} + \frac{1}{\tau_2}\right) = \frac{n_1(L)}{\tau_1}$$